ORIGINAL ARTICLE

Numerical Simulations of Waves Breaking over a Rectangular Submerged Reef Consisting of a Double Step: Analogies with massive Natural Wave Breaking over Abrupt Bathymetries

Florian Desmons[1] · Pierre Lubin[1,2]

Abstract

The aim of this article is not to study any practical design for a breakwater device nor to show the evidence of a particular event when waves break over a varying bathymetry, but to promote a paper showing an interesting idea of wave decomposition prior to impact, used in an experimental and numerical study published by Yasuda et al. (Proceedings 25th international conferences coastal engineering, pp 300–313, 1996) and Yasuda et al. (Coast Eng J 41(2): 269–280, 1999. We investigated the new type of breaker, proposed by Yasuda et al. (1996), by detailing several geometric aspects which lead to the unusual size and behavior of some very large plunging jets generated when waves break above some drastic changes of bathymetry. We thoroughly investigated all geometrical aspects of the breaking process, to propose a classification of the breaker types which were observed in our numerical results. We indicated the influences of the reef parameters (steps heights and lengths) on the subsequent breaking process. We also showed that the air entrainment was indeed much larger during the composite breaker occurrence.

Keywords Numerical simulation · Navier–Stokes · Solitary wave · Step reef · Giant wave

1 Introduction

The coastal waves generated in the deep oceans interact with the lands when they break while reaching the coastlines which are made of various materials (sandy or pebble

---

✉ Pierre Lubin
pierre.lubin@bordeaux-inp.fr

1 CNRS, Arts et Métiers Institute of Technology, University of Bordeaux, Bordeaux INP, INRAE, I2M Bordeaux, 33400 Talence, France

2 School of Civil Engineering, The University of Queensland, Brisbane, QLD 4072, Australia

Birkhäuser

beaches, coral reefs, estuaries, rocky coasts, cliffs, lagoons and wetlands, mangrove forests, etc). Rocky coasts made of submerged parts consisting mainly of cliffs or points/capes/headlands, are often preceded by underwater (and therefore not visible) rock formations on which the waves break (at distances sometimes going to several hundred meters from the shore). Some of these rock formations can be found in forms of rock plates or slabs. Similarly, coral islands are often composed of a lagoon surrounding the submerged and anthropized part of the island. Coastal lagoons are usually connected to the open ocean by inlets, these channels allowing permanent exchanges between the lagoon and the ocean. The coral belt is thus a natural protective barrier against the impacts of the ocean and the waves. Some works found in the literature are dedicated to the study of breaking waves encountered in coastal islands and coral reefs [15–19, 38, 39, 51]. The 2D cross-sections of the system (from offshore to the shore-line) constituted by the coral reef and the lagoon can be schematically represented and modeled as the succession of a flat bottom in deep water (ocean floor), then a more or less steep slope culminating at a maximum point (reef), submerged or not, then a shallow environment, or even again a decreasing slope leading into a shallow basin (see [15–18, 51]). These more or less simplified representations have been used as basic configurations for numerous experimental studies in laboratories for the realization of experiments in hydraulic channels. Yasuda and Hara [52] and Hara et al. [19] performed numerical simulations of solitary waves propagating over submerged rectangular obstacles, considering different sizes and shapes, including the cases of a rectangular step with a vertical face or with a slight slope. The study was designed for practical application, such as breakwater design. Laboratory experiments were carried out by Mayer and Kriebel [39] who considered regular and non-regular wave run-up over non-uniform beach profiles, exhibiting a general concave profile. Several laboratory experiments have been conducted to study the interactions between waves and idealized two-dimensional reef profiles and latter propagation over shallower flat reef-tops [15–18, 38]. More recently, Hsiao and Lin [21], Blenkinsopp and Chaplin [3, 4] investigated experimentally the properties of waves breaking over a submerged reef, idealized as an obstacle exhibiting a front gradient while the rear side drops away vertically from the crest. This geometry was used so that the waves would break in deeper water behind the obstacle.

Numerous problems motivated by fundamental research and applications from environmental and coastal engineering sciences require accurate description of wave breaking [1, 23–25, 31, 45]. A great effort of research is still undertaken concerning wave transformation across the nearshore zone, risk assessments in terms of coastal and ocean structures resistance against periodical waves or tsunamis breaking and effects of turbulence in broken waves on sediment transport. The general knowledge and understanding of turbulence generated by breaking waves has greatly improved in the last three decades. Nevertheless, a lot of work still has to be done in many directions, where some aspects suffer from a lack of efficiency or remaining limitations, such as the capacity of the numerical tools to describe the wide range of length scales present in the breaking process (bubbles, drops and sea spray) and all the physical features (as wind interaction, thermal transfer, gas exchange, dissolution). Indeed, the surf zone is the place where highly complex hydrodynamics occur. Regularly, during the last three decades, important milestone reviews described and commented in

details the general mechanisms involved in the breaking process [42] and the surf zone dynamics [2, 47, 48], while most recent progress have been investigated by [26] and the finest details involved by air entrainment have been described by [10].

One direction of research has consisted in the identification and classification of different types of wave breaking [13]. It is usually admitted that there is a continuous gradation in breaker types from spilling, to plunging, to collapsing and surging. Then, each one of these type of breakers have been thoroughly described and the pre- and post-breaking events needed to be quantified, detected, qualified and classified (in terms of breaking detection, breaker classification, breaker intensity estimation, energy dissipation evaluation, etc.). But no universal scaling laws for physical variables were found so far. Hence, parameterizing breaking effects is still challenging [1, 23–25, 31, 45].

Desmons [11] analyzed and worked to consolidate the knowledge on wave breaking on a flat bottom thanks to numerical simulations, taking advantage of the recent improvements in computer performance which allow the realization of very accurate numerical simulations. The main objective was to analyze the numerical results to improve the description of the initiation of the wave breaking event, in order to be in a situation to better simulate such an event when tackling large coastal areas. Indeed, recent modeling attempts are struggling with the lack of physical knowledge of the finest details of the breaking processes [1, 23, 31].

But when developing or implementing new numerical schemes or methods for simulating free-surface flows [12], comes a time when it is necessary to choose appropriate test cases to verify, validate, assess or showcase the accuracy and tentative improvements brought by the new developments, from simple to more complex configurations. One configuration which comes rapidly to mind, when interested in complex turbulent coastal flows [30], is to consider the propagation and breaking of solitary waves over submerged obstacles, to more complex situations where two solitary waves interact in a head-on collision [37] or a solitary wave impacting a vertical wall [32]. Wroniszewski et al. [50] used the run-up of a solitary wave on a plane beach to benchmark several free available solvers for Navier–Stokes equations, including the numerical tool used by Lubin et al. [36]. Lubin [30] went further in the complexity and closer to our main concern, the breaking waves, in order to validate the numerical model more accurately. The reference case was taken from the work presented by Yasuda et al. [53]. The propagation and the overturning of a solitary wave on a submerged reef, consisting in a rectangular step-like obstacle, was investigated. This test-case allowed to put in evidence the behavior of the wave propagating over a shallow obstacle. Yasuda et al. [53] used a fully nonlinear potential theory model to study the internal velocity and acceleration fields and their relationship to breaker type. They checked the accuracy of their numerical model with some experimental data. We then checked that our numerical model accurately reproduced the propagation and the interaction between the solitary wave and the obstacle [34]. This test-case was also proposed for a benchmark exercise involving several research teams [20].

Therefore, as a start on wave breaking investigation with a more recent version of the numerical tool and newer numerical developments [11], Yasuda's configuration was one of the first to come to mind because we successfully experienced this configuration in the past and many geometric characterizations could be found for

comparisons (plunging jet lengths and thicknesses, angles, surface profiles, velocity and acceleration fields, etc.). Some more research led us to find an older version of the same authors' work [55]. While the more recent version of their work [53] involved a single step reef, interestingly, [55] previously included the use of a reef consisting in a double step, leading to the formation of what was identified as a "new breaker type", consisting in what the authors called a "composite breaker" which particular characteristics was the formation of a "giant plunging jet". They analyzed the efficiency of this new breaker type to dissipate energy, as the massive plunging jet subsequently entrapped more air [54, 55]. Such a breaker was not known nor described before and was supposed to excite strong turbulence by its subsequent impact at the plunge point and cause remarkable dissipation due to larger quantities of air entrapped. Therefore, the authors speculated this particular double-step reef configuration could have led to the development of a new wave control system utilizing a composite breaker. But, Yasuda et al. [55] indicated that this phenomenon of multiple crests interaction was already been observed by Cooker et al. [8]. The study of the latter involved a solitary wave propagating in a 70 m long channel with a single submerged cylindrical bump of semicircular cross-section, placed at the bottom parallel to the incident wave crest. The interaction between the waves and the submerged cylindrical obstacle revealed a variety of forms, depending on the incident wave height and cylinder radius, measured relative to the water depth. Very interestingly, Cooker et al. [8] indicated in the abstract of their paper, that "almost all the resulting wave motions differ from the behavior which was anticipated when the study began". They reported a number of new phenomena, the most interesting one concerning our study being the generation of a double crest when the wave interacts with the obstacle. They reported that all solitary waves of amplitude greater than about 0.2, riding over cylinders larger than about $R = 0.5$ (non-dimensional radius used by Cooker et al. [8]), exhibited a double crest as they crossed the obstacle. The incident wave approached the submerged obstacle and a bulge grew in the surface, on the opposite side of the obstacle. The bulge grew into the crest of a new wave, which propagated away from the obstacle. While the new crest grew, the incident crest decayed to a fraction of its original height, and slowed down. Then its direction reversed and it propagated away as a small reflected wave. They called this effect "crest-crest exchange" because "the wave appears to exchange one crest for another in a short period of time" [8]. It should be noted, however, that no breaking event was subsequently reported for the "crest-crest exchange" regime in their study. Therefore, Yasuda and Hara [52] investigated further this particular phenomenon, with the particular feature that the "crest-crest exchange" ends-up in the addition of both crests at the plunging jet's generation, resulting in what has been observed as larger than the usual jet size, the so-called "giant jet".

Intrigued by the mention of this new type of breaker [55], which we never heard of before, we checked that, to the best of our knowledge, if this work had ever been used or cited to eventually have more information. Surprisingly, this work remained somehow confidential, mainly cited later by the same authors in extended works with no more details [3, 4, 19, 33, 40, 53–55]. It has to be mentioned that Mutsuda and Yasuda [40] extended the experimental 2D configuration to a 3D numerical study, leading to one of the earliest numerical results for the three-dimensional Large Eddy Simulations of a plunging breaking wave [30, 36]. This intrigued and led us to consider this fascinating

configuration as a strong candidate for an extended numerical investigation. As we will later discuss, some articles have detailed the solitary wave fission process generated by its propagation over a single submerged step, but the beauty of Yasuda's work was to induce a so-called composite breaker by decomposing the incident solitary wave in two waves which celerities imply that both will sum up at the plunging jets initiation, generating a so-called giant plunging breaker.

To summarize, Yasuda et al. [55] identified that:

(i) due to the interaction between the incident solitary wave and the first step, an instability is triggered and develops, in a form of a triangular-shaped crest appearing at the free-surface on the back of the propagating solitary wave;

(ii) the triangular-shaped peak develops rapidly (so-called "fast-growing"), propagates in the same direction as the main wave, towards the shallow part of the reef, and eventually catches up the crest of the incident wave;

(iii) both crests compose together at the breaking point to form a larger than normal plunging jet ("giant jet").

But we must mention that, in later works, [54] studied the composite breaker, but did not mention the triangular-shaped crest nor the crests exchange mechanism.

The objective of this paper is thus not to demonstrate the interest of a numerical model, nor the superiority/novelty of our numerical methods, but to recall a crucial study, yet to be spread to a larger audience. These results, underrated for no apparent reason, apart maybe for lack of further elements which could improve the description and later analysis. Many articles can be found for multiple forms of underwater obstacles. But, to the best of our knowledge, no such composite reef, compound with two rectangular steps. We thus conducted a series of 22 two-dimensional Direct Numerical Simulations (DNS) of solitary waves propagating and breaking over a reef consisting of two steps, mimicking the experimental configuration proposed by [55], to investigate these three aspects of the experimental observations: triangular-shaped crest formation, development of this free-surface deformation leading to the generation of a "giant jet" as both crest add up when plunging breaking. We will then analyze the geometric characteristics of the final plunging jet prior to impact, and the subsequent air entrainment. A discussion about the possible analogies for large notable breaking waves made famous for surfing will be proposed to conclude the article.

2 Numerical Simulation Details

2.1 Model and Numerical Methods

The aim of the present work is to numerically explore the two-dimensional behavior of a breaking wave influenced by stepped bathymetry. Solving of incompressible Navier–Stokes equations (Eq. 2.1) coupled with a Volume-of-Fluid interface representation method (Eq. 2.2) has already proven its effectiveness to study the pre- and post-impact dynamics [11, 12, 33]. Therefore, all simulations were carried out using the same framework and algorithm from Desmons [11] and Desmons and Coquerelle [12]. The interaction of the wave and the bathymetry, represented by a non-porous solid, is taken into account by a penalization method:

$$\begin{cases} \frac{\partial \rho \mathbf{u}}{\partial t} + \nabla \cdot (\rho \boldsymbol{u} \otimes \boldsymbol{u}) = -\nabla p + \rho \boldsymbol{g} + \sigma \kappa \nabla C + \nabla \cdot (\mu (\nabla \boldsymbol{u} + \nabla \boldsymbol{u}^T)) \\ \nabla \cdot \mathbf{u} = \mathbf{0} \end{cases} \quad (2.1)$$

$$\frac{\partial C}{\partial t} + \mathbf{u} \cdot \nabla C = 0 \quad (2.2)$$

with ρ the fluid density, $\mathbf{u}$ the fluid velocity, p the pressure, $\mathbf{g}$ the gravitational vector, σ the surface tension coefficient, κ the local interface curvature, C the color function representing the ratio of one phase into each cell and μ the fluid viscosity.

The massively parallel open-source software Notus[1] CFD is used for simulating the breaking event, solving the equations on Cartesian staggered grids within a finite volume method framework. The couple velocity–pressure is evaluated through time by solving the Eq. (2.1) using a prediction-correction method [14]. The surface tension is evaluated with the Continuum Surface Force (CSF) model developed by [5] and under the well-balanced method proposed by Popinet [44]. The local interface curvature κ is represented thanks to the color function of the Volume-of-Fluid interface representation method using a combination of two height function algorithms [41, 43]. The viscosity term is computed with an Euler implicit temporal scheme and a second order spatial scheme. The advection term is computed with an explicit 3-stage 2nd-order Runge Kutta type scheme (NSSP32) and a WENO3 spatial scheme. The OpenMPI library is used to parallelize the code and the mesh is partitioned into equal size subdomains to ensure load balancing. The HYPRE parallel solver and preconditioner library is used to solve the linear systems. Desmons and Coquerelle [12] extensively detailed the numerical methods and thoroughly verified and validated the numerical tool through numerous test cases. The 2D numerical domains are partitioned into 320 subdomains (one processor per subdomain). On average, each simulation ran for 60 h of computing time.

2.2 Initial Conditions and Reef Geometry

A solitary wave is initialized in a rectangular two-dimensional numerical domain (Fig. 1). The free-surface profile, the velocity and pressure fields are initially calculated with the theoretical first order solitary wave solution [27, 30]. The solitary wave propagates towards the right side of the numerical domain, from the flat uniform bed towards the double-step reef located at the right end side of the numerical domain. The initial position of the crest of the wave is taken at $x_{crest} = 2.6$ m, which was verified to be far enough from the reef position in order to minimize its influence on the breaking event. Furthermore, the initial wave height was slightly overestimated in order to ensure the targeted wave height $H_1 = 0.155$ m corresponding to the one observed in Yasuda's experiments before the wave interacts with the reef. The still water depth is $h_1 = 0.31$ m, while the still water depth in the shallower part of the domain, above the last step, is $d = 0.047$ m.

The reef is composed by a combination of two steps bound to each other (Table 1). The highest one, which is $R_1 = 0.248$ m will remain constant for all presented simulations, is set at the position $x = 8.1$ m from the left boundary. The second step

---

[1] Notus CFD code: http://www.notus-cfd.org is developed in the I2M Laboratory.
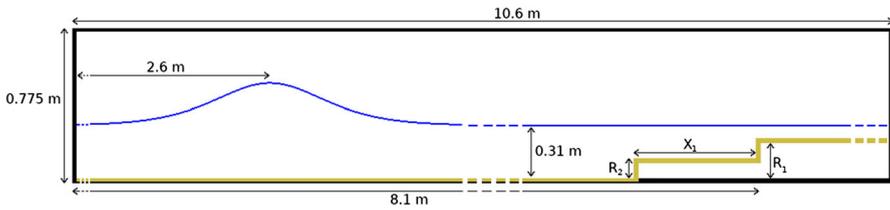
Fig. 1 Initial condition with R_1 the fixed first step height, R_2 the second step height and X_1 the distance between the two steps

Table 1 Physical parameters used for the numerical simulations

Water density, ρ_w	1000 kg m^{-3}	Water viscosity, μ_w	1×10^{-3} kg m^{-1} s^{-1}
Air density, ρ_a	1.1768 kg m^{-3}	Air viscosity, μ_a	1.85×10^{-5} kg m^{-1} s^{-1}
Gravity, g	9.81 m s^{-2}	Surface tension coefficient, σ	0.0728 N m^{-1}
Initial wave amplitude, H_1	0.155 m	Initial wave celerity, c_1	2.34 m s^{-1}
Initial water depth, h_1	0.31 m		

Initial solitary waves quantities are calculated thanks to the 1st order solution [27, 35]

height R_2 is modified during the numerical study. It is set at a distance X_1 before the first step. The interactions between the incident wave with this combination of steps is responsible for generating a complex behavior leading to the breaking event. It has to be noted that, in order to remain consistent with Yasuda et al. [55] and Yasuda et al. [54], we keep the same notations throughout the whole study. The values for the different parameters are summarized in Tables 2, 3 and 4.

The left, bottom and top boundaries are set with a wall condition. Moreover, as small damping layer has been set at the left boundary in order to reduce the spurious instabilities coming from the initialization and reflecting on the left wall. The right boundary is set as a homogeneous Neumann condition to minimize the domain limit influence on the fluid motion.

The spatial steps are set constant all over the domain, with $\Delta x = 8 \cdot 10^{-4}$ m and $\Delta y = 7.75 \cdot 10^{-4}$ m for a total size of mesh of: $13,250 \times 1000 = 13,250,000$ cells. These values were taken in order to synchronize the mesh with the reef geometry and increase the order of the penalization method. Furthermore, they were found to be a good compromised between the time calculation, more especially under the surface tension constraint, and the accuracy of the breaking behavior over the composed reef.

2.3 Experimental Configuration Discussion

Yasuda et al. [53] used a single step reef to observe and investigate plunging and spilling breaking waves. First, the wave propagated over the flat bottom without any change of form. Then, when it arrived in the neighborhood of the obstacle, the water depth over the reef abruptly reduced, which led the wave profile to be dramatically transformed. The wave was then forced to reorganize itself. As recorded by the gauge standing over the reef's upstream corner, the free-surface elevation increased from the

Table 2 Numerical simulations parameters. Initial water depth in front of the reef is set at $h_1 = 0.31$ m

R_2 (m)	0.093	0.124	0.155	0.186
X_1 (m)	0.31	0.31	0.139	0.248
	0.62	0.62	0.31	0.62
	2.17	1.24	0.93	0.93
	3.10	2.015*	1.395	1.085
	4.03	3.10	1.55	1.24
			2.015	1.4

While the height of the second reef step is kept constant at $R_1 = 0.248$ m, we performed 22 numerical simulations with different heights R_2 for the first step of the double reef and lengths X_1 between the two steps

()*Reference configuration from Yasuda et al. [55]

initial value. The wave lost its symmetrical aspect and started steepening till the front face of the crest became vertical before eventually breaking. It also highlighted the fission phenomenon: when solitary waves propagate from deep water into shallower water, the incoming waves disintegrate into two or more solitons. This was already explained analytically [49] and more closely studied and illustrated numerically and experimentally [7, 9, 22, 28, 29, 46], for breaking and non-breaking cases. Given the initial conditions (i.e., the mean water depth, the amplitude of the incoming solitary wave and the height of the obstacle), the amplitude and the number of the transmitted waves could be predicted, as well as the amplitude of the reflected wave. Yasuda and Hara [52] indeed also studied this aspect of the process earlier when investigating breaking and reflection as the solitary wave interact with the submerged step. Then Yasuda et al. [55] used the double reef, which heights were set at $R_1 = 0.263$ m and $R_2 = 0.131$ m for the upper and lower crowns respectively. The distance X_1 between the first and second steps was changed from 0.0 to 2.5 m, while the situation where $X_1 = 0.0$ m, the second step R_2 vanishes, and the reef only consists in fact in a single reef configuration.

The difference between the solitary wave propagating on a single step [53] is that in the case of a double step, the wave stumbles/trips while it hits the R_2 step, then deforms as it keeps on propagating towards the next higher R_1 step, resulting in the generation of an instability developing in a visible triangular-shaped crest appearing above the main wave (see photo 1 in Yasuda et al. [55]).

In the case of a double-step configuration, Yasuda et al. [55] concluded that the new breaker type, referred to as a composite breaker, was characterized by the formation of a so-called giant jet which was generated by the composition of a near-breaking incident crest and a fast-growing 2nd crest. The reciprocal effect formed a triangular crown and produced a giant jet by incorporating the triangular crown into the 2nd crest. Yasuda et al. [54] pursued the study and highlighted some of their earlier results, but some differences should be pointed out. As presented in Table 3, Yasuda et al. [55] and Yasuda et al. [54] presented almost the same values for the experimental, except the non-dimensional step height $\dfrac{R_1}{h_1}$. Yasuda et al. [55] used $\dfrac{R_1}{h_1} = 0.8$ and $R_1 = 0.263$ m,

Table 3 Initial laboratory experimental configuration setups, used and to be compared

References	Breaker type	h_1 (m)	$\dfrac{H_1}{h_1}$	$\dfrac{d}{h_1}$	$\dfrac{R_1}{h_1}$	$\dfrac{R_2}{h_1}$	X_1 (m)
Yasuda et al. [55]	Composite	0.31	0.50	0.15	0.8	0.423	from 0.0 to 0.1
Yasuda et al. [54]	Composite	0.31	0.50	0.15	0.85	0.43	0.806
This study	Composite	0.31	0.50	0.15	0.8	See Table 2	See Table 2

while Yasuda et al. [54] mentioned $\dfrac{R_1}{h_1} = 0.85$ but did not specify the dimensional value for R_1. If we evaluate 0.263/0.31, we get $\dfrac{R_1}{h_1} = 0.848387$. If we check Yasuda et al. [55], using $\dfrac{R_1}{h_1} = 0.8$ we get $R_1 = 248$ m, which is different from the value given in Yasuda's paper from 1996. If we check Yasuda et al. [54], using $\dfrac{R_1}{h_1} = 0.85$ we get $R_1 = 0.2635$ m, which is not verified in Yasuda's paper from 1999 and still different from the 1996 paper. We assumed that Yasuda et al. [55] rounded $\dfrac{R_1}{h_1} = 0.848387$ to the first decimal $\dfrac{R_1}{h_1} = 0.8$, while Yasuda et al. [54] rounded $\dfrac{R_1}{h_1} = 0.848387$ to the second decimal $\dfrac{R_1}{h_1} = 0.85$. As all the results are presented in dimensionless form, we chose to use $\dfrac{R_1}{h_1} = 0.8$ to evaluate R_1 which we set at $R_1 = 0.248$ m, this allows us to compare well our result qualitatively, as presented in the following sections.

The extreme angle of the first vertical step creates instant instability in the wave. The second stage of the reef, consisting of a horizontal flat reef extending along the X_1 distance, proceeds uniformly until the wave hits the second vertical step. The last stage of the reef is the shallower flat reef top. The wave is deformed when hitting the step of height R_2, but does not steepen enough to break in most configurations (see Table 4). The height R_2 is not enough to make the incident solitary wave to stumble and break in the vicinity of the step, but the wave is destabilized and starts to deform as it looses its symmetrical aspect as it is slowing down while it tries to reorganize itself. So the modified wave keeps propagating towards the next step, along the X_1 distance until it reaches the last step of height R_1, which is able to move suddenly upwards a larger portion of the wave. This leads to a much pronounced deformation of the wave, which then steepens until the front face of the wave is vertical.

The incident crest turned to reveal a triangular form and its height exceeded that of the breaker on a single reef, as the relative step distance X_1/h_1 increased. However, when the value of X_1/h_1 exceeded about 7.0, a small jet was ejected from the incident crest before the incident crest got to be combined with the 2nd one and then a giant jet was formed. We qualified this breaker as a multiple breaker (see Figs. 2b, and 3a–g, and Table 4).

Table 4 Non-dimensional parameters for the 22 numerical simulations

$\dfrac{R_2}{h_1}$	$\dfrac{X_1}{h_1}$	Breaker type	Observations
0.3	1.0	Regular plunging breaker	
	2.0	Regular plunging breaker	See Fig. 5
	7.0	Composite breaker	
	10.0	Composite breaker	
	13.0	Multiple breaker (see Figs. 2b, and 3a–g)	
0.4	1.0	Regular plunging breaker	
	2.0	Regular plunging breaker	See Fig. 5
	4.0	Composite breaker	
	6.5	Composite breaker—reference configuration from Yasuda et al. [55]	See Fig. 2a
	10.0	Multiple breaker	
0.5	0.45	Regular plunging breaker	
	1.0	Regular plunging breaker	
	3.0	Composite breaker	
	4.5	Composite breaker	
	5.0	Composite breaker	
	6.5	Multiple breaker	
0.6	0.8	Regular plunging breaker	See Fig. 4c
	2.0	Composite breaker	See Fig. 5
	3.0	Composite breaker	
	3.5	Composite breaker	
	4.0	Composite breaker with the largest plunging jet tip at impact	See Fig. 4b
	4.52	Multiple breaker	

3 Results' Analysis and General Discussion

Unfortunately, Yasuda et al. [55] presented no experimental pictures giving information about the abscissa of the jet impact or the splash-up behavior. We also missed time information, which prevent us to compare quantitatively our results to the experimental pictures. However, our numerical results fit very well with the observations of Yasuda et al. [55] considering the wave breaking initiation phenomenon and the subsequent processes, as later described. However, we aim at exploring the three main features described by Yasuda et al. [55], naming the generation of a triangular crest, its fast-growing development and its composition with the incident wave crest leading to the formation of a so-called giant jet. So our results will be described in the following sections, as a function of the different combinations of heights R_2 and lengths X_1, keeping R_1 fixed as in Yasuda et al. [55].

3.1 New Crest with Triangular Shape Crown

In order to illustrate this feature of the process, we present pictures from our numerical simulation of the exact same configuration to the one shown by Yasuda et al. [55]. The picture shown in Fig. 2a presents the time evolution of the free-surface profiles of the incident solitary waves propagating over the double reef, up to the impact of the plunging jet, with the early stage of the splash-up generation. Due to the interaction between the incident solitary wave and the R_2 step, the incident solitary wave adapts to the shallower water depth above the R_2 step, the wave crest rises in height, in a form of a triangular-shaped crest. It can be clearly seen in Fig. 2a that the free-surface is modified, exhibiting a large kink which is observed to grow in size on top of the propagating wave (see third profile right above the last step at $X_1/h_1 = 38$), which then meets the next step leading to the general overturning process. The triangular-shaped crest decays in size, while the front face of the propagating wave starts bulging and steepening until it becomes vertical (generating another crest—see sixth profile)). It then ejects a jet at the top of the second crest (at $X_1/h_1 = 40$ as also found in Fig. 7 by Yasuda et al. [55]), where at the same instant and at the same location the decaying triangular-shaped crest comes to participate in the general overturning process. A large jet is observed to overturn and impact at $X_1/h_1 = 42$, larger to what usually experienced (see further discussions).

The wave profiles shown in Fig. 2a are very similar to those presented by Yasuda et al. [55] (see Figs. 6, 8 and 11 showing numerical and experimental profiles of the evolution of the composite breaker).

3.2 Fast-Growing Triangular Crest

This aspect was not very clear to us when reading the paper from Yasuda et al. [55]. They mentioned that the triangular-shaped peak develops rapidly ("fast-growing") and propagates in the same direction as the main wave, which propagates towards the shallow part of the reef. As previously shown in Fig. 2a, the incident wave first hits the R_2 step, which initiates the modification process of the solitary wave propagating in a shallower depth (which is the mean water depth minus the R_2 step height). The incident solitary wave looses its initial symmetrical aspect, leading to the triangular crown described previously. If the R_1 step would not have been there, this R_2 step involves that the incident solitary wave would have evolved as it would slowly start the steepening process preceding the breaking event when reaching an unstable height. On the fourth wave profile, we can see the triangular-shaped crest decaying in size, while the second crest, generated by the encounter of the next R_1 step, is forming ahead of the wave front, leading to the presence of two crests visible on the fifth profile. The sixth profile allows presenting both crests which participate in the breaking, the triangular-shaped on top of the second one, which is not the highest point of the wave profile, but where we feel the birth of the jet about to be ejected as clearly visible on the seventh profile.

In Fig. 3a–g, we present the free-surface profiles for a lower height R_2 and a greater length X_1. It can be observed that we obtained multiple breaking events due to the
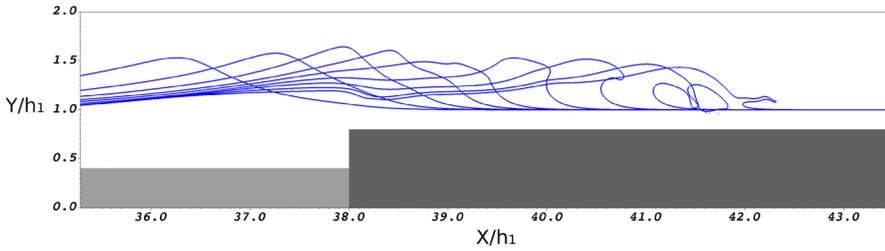
(a) $R_1/h_1 = 0.8$, $R_2/h_1 = 0.4$ and $X_1/h_1 = 6.5$. This can be compared to the picture shown in figure 7 by Yasuda *et al.* (1996).
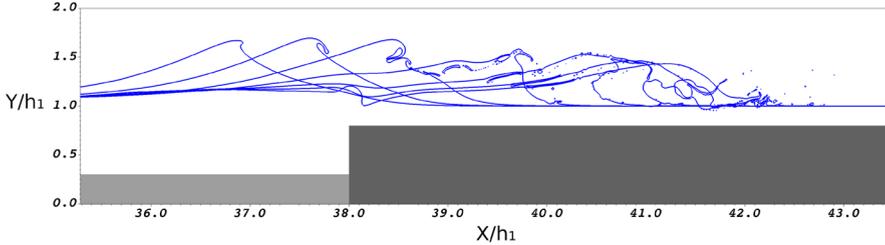
(b) $R_1/h_1 = 0.8$, $R_2/h_1 = 0.3$ and $X_1/h_1 = 13$. We obtained multiple breaking events with this configuration. This configuration is detailed in the following figure (see Fig. (3a) to (3g)).
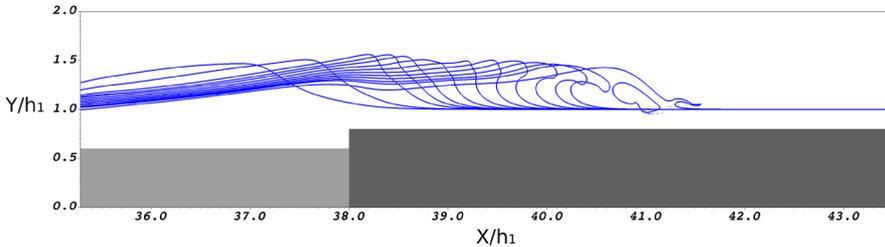
(c) $R_1/h_1 = 0.8$, $R_2/h_1 = 0.6$ and $X_1/h_1 = 4$. We obtained the largest plunging jet with this configuration.
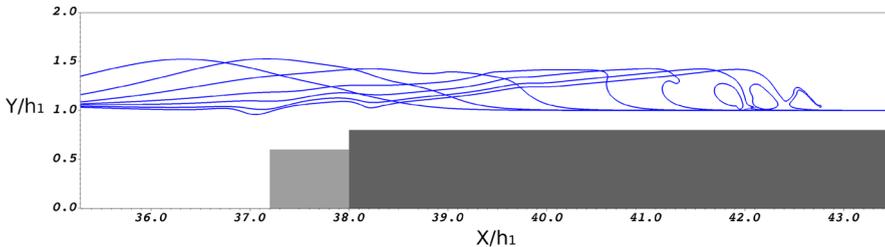
(d) $R_1/h_1 = 0.8$, $R_2/h_1 = 0.6$ and $X_1/h_1 = 0.8$. We obtained a much classical plunging jet with this configuration.

Fig. 2 Time evolutions of the free-surface profiles of the incident solitary waves propagating over the double reef, up to the impact of the subsequent plunging jets, with the early stages of the splash-up generations. R_1/h_1 is kept constant and varying R_2/h_1 and X_1/h_1
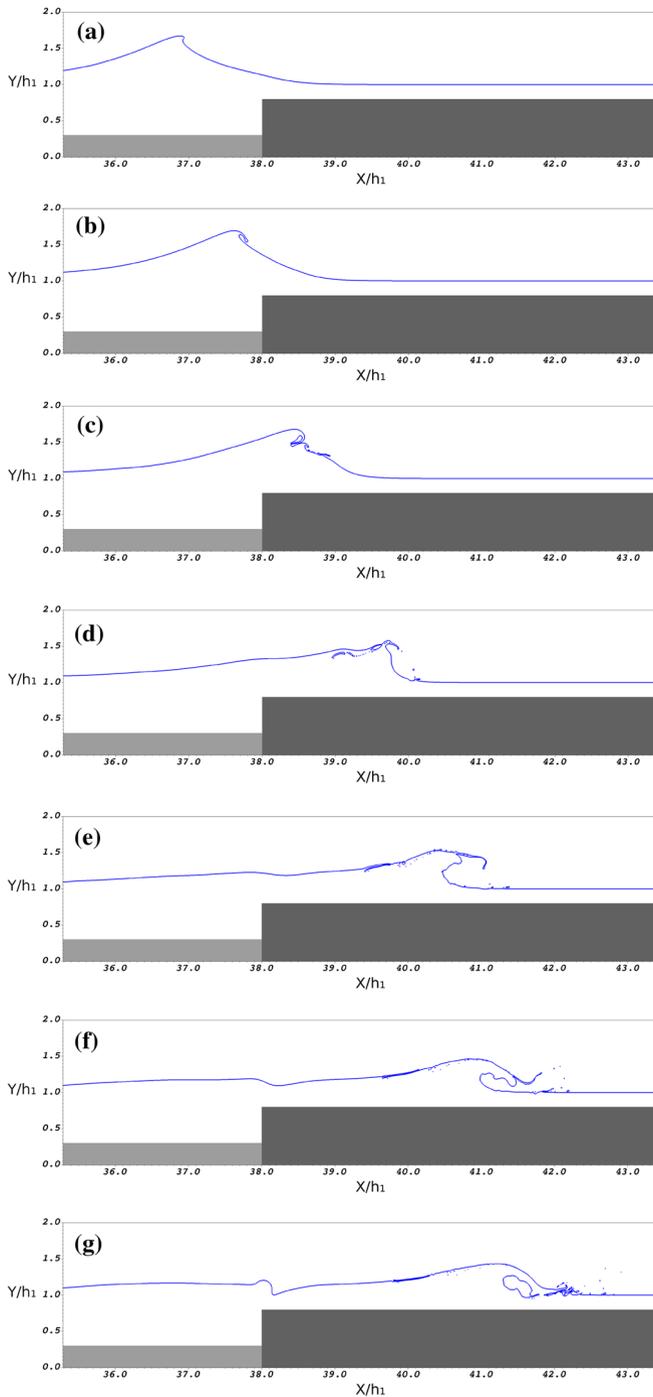
Fig. 3 Time evolutions of the free-surface profiles of the incident solitary waves propagating over the double reef, up to the impact of the subsequent plunging jets, with the early stages of the splash-up generations. $R_1/h_1 = 0.8$, $R_2/h_1 = 0.3$ and $X_1/h_1 = 13$

two crests evolving separately. On the first profile (Fig. 3a), the triangular-shaped crest finally becomes unstable and overturns as a weak plunging breaker, exhibiting a small jet ejection at the very top of the propagating wave (Fig. 3b), which has not reached the next step yet. Then, the still propagating wave hits the final step, and deforms while its upper part is already breaking (Fig. 3c). Another crest starts to grow from the front face (Fig. 3d), carrying the previous breaking event and the subsequent air entrapment. As it rises and propagates towards the right side of the domain, a final breaking plunging event is generated (Fig. 3e), merging with the successive splash-ups from the first breaking event still active on the top of the wave, leading again to the formation of a "giant jet" (Fig. 3f), entraining much more air in the water (Fig. 3g). This feature was also observed by Yasuda et al. [55] for X_1 larger than 0.7, which is in accordance with our observations.

We present in Fig. 2c a situation with the same length X_1 as previously, and increasing R_2 close to the height of the last step R_1. It can be seen that no triangular-shaped crest is generated, as in the previously described configuration, but the final plunging jet is still very large. The R_2 step generates the modification of the incident solitary wave which starts to steepen but eventually hits the following R_1 step provoking an increase in height of the front face (see the seventh profile), where the two crests merge to form a bulge leading to one of the largest plunging jet we experienced. On the seventh free-surface profile, it can still be seen that a small triangular crown is located on top of the rising bulge, so proving the existence of the two crests exchange mechanism leading to the composite breaker eventually breaking.

We present in Fig. 2d a situation with a higher R_2 (close to the height of the last step R_1) and a shorter X_1. It can be clearly seen that no triangular-shaped crest is generated, and thus no larger than usual plunging jet is observed. It can also be noted that the breaking point is the farthest presented in this paper, the breaking event being delayed. But still, on the third profile two humps can be observed, leading to a long flat crest presented on the fourth profile. The first hump (left side) is in fact the crest of the previous second profile which is decaying in height, while the first on the right side is growing from the next step encounter, leading to the crest observed in the fourth profile, being the highest point of the wave profile.

3.3 Giant Jet Generated by the Combination of the Two Crests

As described previously, the incident wave is impacted by the two submerged steps, which induces that the incident wave will experience the evolution to the breaking process two times. The first time, it can generate the triangular-shaped crest (see previous descriptions), then the wave hits the next step, $R1$, being much higher, forcing the wave to rapidly overturn. Both crests compose together at the breaking point to form a larger than normal plunging jet ("giant jet").

It can be seen that the shorter the distance X_1 between the two steps is, the more "classical" the plunging jet is. As seen in Fig. 2d, no triangular-shaped crest is visible, so no crests' combination (or crest-crest mechanism as described by Cooker et al. [8] and Yasuda et al. [55]) occurs, resulting then in a plunging jet of regular size, ejected from the highest crest of the steepening wave. In the case of a single step, we mentioned

that the solitary wave is seen to experience the fission phenomenon: the wave is separated in two parts, one being reflected and going backwards, while a transmitted part will keep on propagating. In the two steps configuration, the transmitted part will experience another fission. It can even be seen in Fig. 2d that, whatever the size of the R_2 step, the decaying first crest remains far behind the steepening vertical front of the near-breaking wave, as it is separated from the wave propagating after passing over the last step.

In order to investigate further this "larger than usual jet", we propose to look at some comparisons, presented in the following figures. We show in Fig. 5 three wave profiles when the waves are about to break, for different values of R_2, keeping R_1 and X_1 constant. It can be seen that all the wave profiles look very similar, all the wave heights are the same, and the higher R_2 is, the faster the wave is breaking. Indeed, the wave profile for the lower R_2 is observed to become vertical farther than the wave profile for the higher R_2. The crest exchange mechanisms are similar, the first crests all decay at the same location while the second crest rises at the same heights but at different abscissas.

In Fig. 4a, we present the same two situations, but further in time, when the jets have been ejected and started the overturning motions. It can be seen that the longer X_1 is, the bigger the plunging jet is. Also, the longer X_1 is, the higher the wave profile is. For the higher X_1, the wave profile exhibits a small triangular-shaped crown which is above the second crest rising from the R_1 step encounter. For the lower X_1, no triangular crown is observed on top of the second crest, and the wave profile exhibits a long plateau between the crest overlooking the vertical face of the wave and the hump located at $X_1/h_1 \simeq 39.4$.

In Fig. 4c, we present again the same two situations, but the jets are about to impact. It can be seen that the longer X_1 is, the longer the plunging jet is. The air cavity which is about to be entrapped at the impact is thus larger than when X_1 is shorter. It can also be noted that the tip of the long free-falling plunging jet is slightly bent prior to impact. It will be discussed in the next section (3.4) that it is not an effect of the interaction with the surrounding air flow. This has also to be compared with the situation where X_1 is shorter: the aspect of the free-falling plunging jet does not exhibit such an inflexion.

3.4 Geometrical Characteristics of the Plunging Jet and Subsequent Air Entrapped

While Yasuda et al. [55] detailed the "giant jet" characteristics by analyzing the associated geometrical quantities, we thus analyzed further our numerical results to show that the presence of the triangular-shaped crown not only led to a larger than usual plunging jet as it adds to the final jet ejection when the incident wave finally breaks in the shallower part of the domain, but it also modifies the overall aspect of the free-falling jet once ejected from the crest of the breaking wave.

The geometrical characteristics investigated and discussed through this paper are introduced in Figs. 6 and 7.
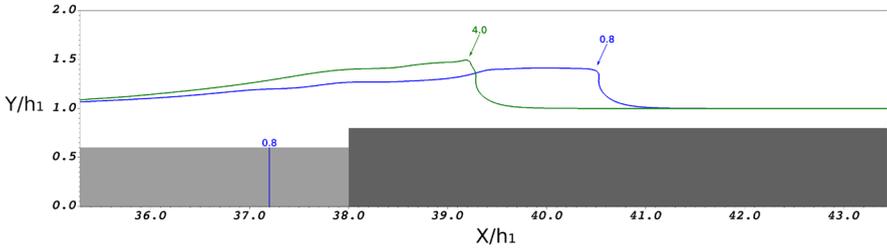
(a) Comparisons of the solitary wave profiles leading to a composite breaker on a double reef, for $R_1/h_1 = 0.8$, $R_2/h_1 = 0.6$ and varying $X_1/h_1 = 0.8$ (blue line) and $X_1/h_1 = 4.0$ (green line). We compare the wave profiles prior to the jets' ejections.
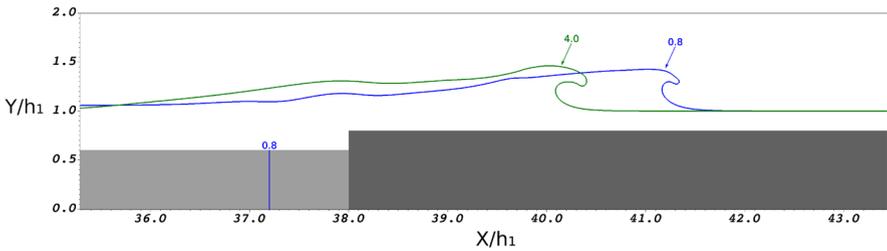
(b) Comparisons of the solitary wave profiles leading to a composite breaker on a double reef, for $R_1/h_1 = 0.8$, $R_2/h_1 = 0.6$ and varying $X_1/h_1 = 0.8$ (blue line) and $X_1/h_1 = 4.0$ (green line). We compare the wave profiles when the plunging jets are overturning.
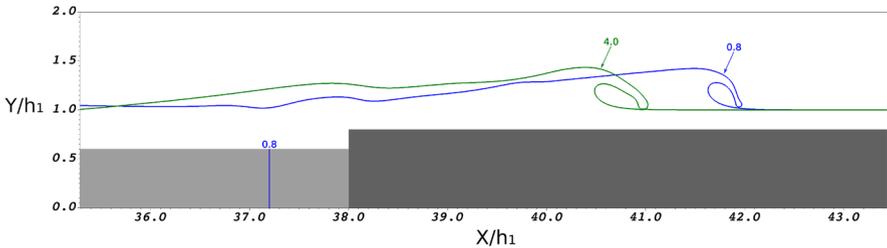
(c) We compare the wave profiles when the jets are free-falling down to the breaking impact points.

Fig. 4 Comparisons of the solitary wave profiles leading to a composite breaker on a double reef, for $R_1/h_1 = 0.8$, $R_2/h_1 = 0.6$ and varying $X_1/h_1 = 0.8$ (blue line) and $X_1/h_1 = 4.0$ (green line) (color figure online)

3.4.1 Roller and Subsequent Aeration

In Fig. 8, we present the evolution of the characteristics related to the roller as a function of $\frac{X_1}{h_1}$ for $\frac{R_2}{h_1} = 0.3,\ 0.4,\ 0.5$ and 0.6. It can be seen that the R_2 step height and the X_1 length influence the behavior of the roller prior to impact.

The roller length L_R is a characteristic mainly influenced by the configuration of the step. It can be observed in Fig. 8a the increase of its value regarding the distance between the steps, but also the second step height R_2. And more especially for $\frac{X_1}{h_1} > 2.25$ which corresponds to a breaking behavior coming from the composite
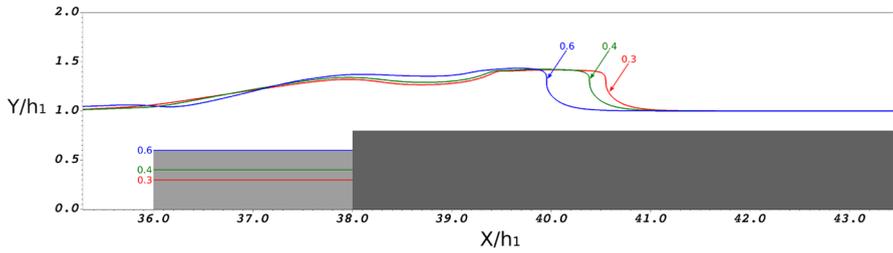
(a) We compare the wave profiles prior to the jets' ejection. For a fixed length between the first and second steps, the higher the R_2 step, the faster the breaking event occurs.
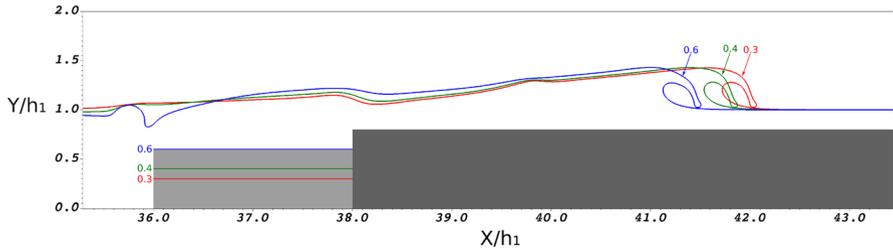
(b) We compare the impacting jets locations as a function of the R_2 step's height.
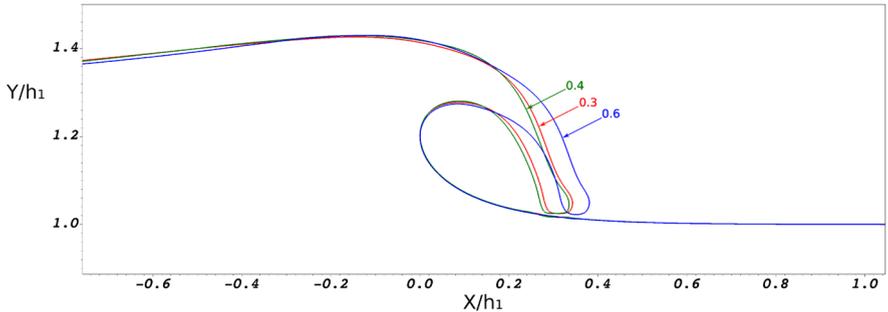
(c) We compare the sizes of the pockets of air entrapped by the plunging jets, as a function of the R_2 step's height. The wave profiles have been shifted along the longitudinal axis, so that their positions all coincide to allow a comparison of their respective plunging jets.

Fig. 5 Comparisons of the solitary wave profiles leading to a composite breaker on a double reef, for $R_1/h_1 = 0.8$ and $X_1/h_1 = 2.0$ fixed, and varying $R_2/h_1 = 0.6$ (blue line), $R_2/h_1 = 0.4$ (green line) and $R_2/h_1 = 0.3$ (red line) (color figure online)

breaker, as described by Yasuda et al. [55] (X_1 larger than 0.7). In fact, this increase in the roller length L_R is coming from the interaction between the multiple breaking event generating a jet impacting the free-surface in a higher distance, reducing in the roller impact angle (see Fig. 8c). The longer the jet distance, the lower the roller angle, α_R.

Due to the two crests interaction, generated from the second and first steps, a bump is generated and transported with the jet and so inside the roller. This bump creates a jet composed by two smaller jets with different angles and widths. The evolution of this bump inside the roller is directly influenced by the R_2 step characteristics, which
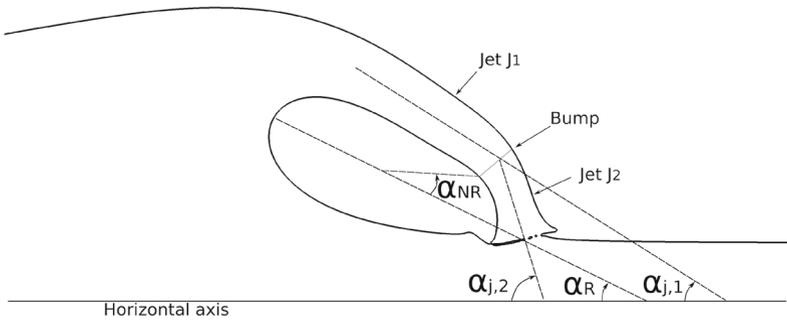
(a) Definition sketch of the characterized angles at the impact moment : α_{NR} the angle of the bump inside the roller, α_R the roller impact angle, $\alpha_{j,1}$ the first jet J_1 angle and $\alpha_{j,2}$ the second jet J_2 angle.
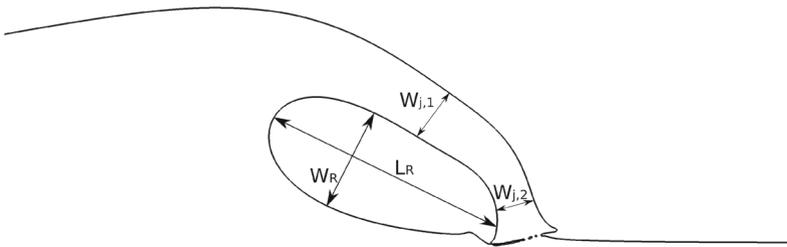
(b) Definition sketch of the characterized lengths at the impact moment : L_R the length of the roller, W_R the roller width, $W_{j,1}$ the first jet width and $W_{j,2}$ the second jet width.

Fig. 6 Definition sketch for the geometrical properties evaluated for the plunging jet prior to impact
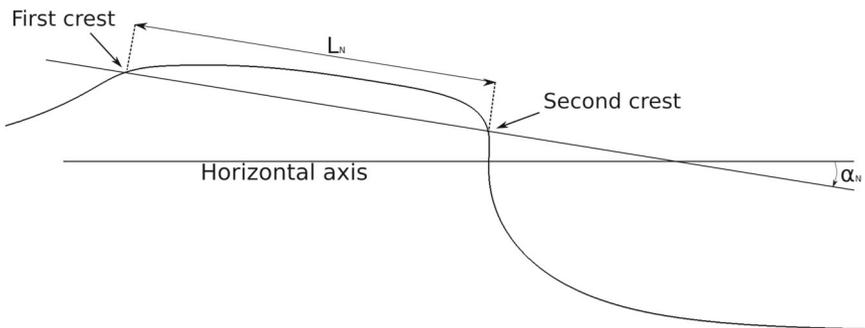
Fig. 7 Definition sketch for the geometrical properties evaluated for the plunging jet prior to starting point : L_N the length between the first and second crest and α_N the angle generated by the two crests

modify the global aspect of the roller, as it can be seen in Fig. 8b where the roller width is increasing with the steps distance. In fact, this modification is mainly coming from the bump generating a higher roller width, but only when the bump is far enough from the impact point. When the bump angle inside the roller is under 40° (see Fig. 8d) the roller width tends to decrease.

In Fig. 8a, c and d, for a small distance X_1 all of the results obtained are close to each other. Hence, the influence of the R_2 step geometry can be neglected and the breaker type observed is close to a regular breaker. The breaking waves with a roller length $L_R < 0.11$ m, a roller angle $\alpha_R > 40°$ and a bump angle $\alpha_{NR} > 100°$ are defined as regular breakers while the others are defined as composite breaker (see Table 4).

The roller, with an increase in length L_R and slight increase in width W_R, due to the composite breaker can grow up to more than 60% the area of air entrapped during the impact of the jet in comparison of a regular breaker (see Fig. 8e).

3.4.2 Impacting Jet

The impacting jet can be separated into two smaller jets due to the bump generated by the interactions with the multiple breaker. The upper jet J_1 impact angle increases as the second step becomes longer and higher (see Fig. 9a). Except for $\frac{R_2}{h_1} = 0.3$, the jet width $W_{j,1}$ tends to increase slightly or remains relatively constant (see Fig. 9b). The lower jet angle $\alpha_{j,2}$ increases slightly with the steps distance. But its width is increasing following the step length and height (see Fig. 9d).

For a "regular breaker" the jet width tends to reduce with time until the impact point, creating a fine jet, as commonly observed in the literature. This behavior can be seen at Fig. 2d. On the contrary, the jet generated for a multiple breaker has a quasi-constant width, generating a massive jet impacting the surface. This second behavior can be seen on Fig. 2c. It can be explained by an increase of the lower jet width $W_{j,2}$ which becomes closer to the upper one and also by a longer upper jet. The closer the bump inside the roller to the impact point, the longer the upper jet will be, which is the thicker one. Moreover, the interaction of the two breaking generates a jet going farther than for a "regular breaker" (see Fig. 5c). These characteristics generate an impression of a giant jet.

In the Fig. 9d for a small distance X_1 all of the results obtained are close to each other. Hence, the influence of the R_2 step height can be neglected, and the breaker type observed is close to a regular breaker. The breaking wave with a lower jet width $W_{j,2} < 0.014$ m are defined as regular breaker, while the other are defined as composite breakers (see Table 4).

3.4.3 Characterization of the Two-Crest Behavior

During the initial stage of the breaking event, when the wave surface becomes vertical, the influence of the R_2 step generates a first crest close to the one that will be generated by the R_1 step. The R_1 crest, in most of our simulations, is higher than the second one ($\alpha_N < 0°$). Both characteristics, the angle α_N and the distance between both crests L_N, are highly influenced by the R_2 step height (see Fig. 10).
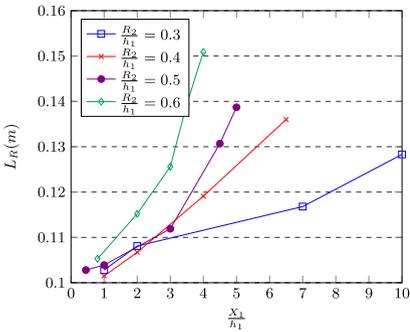
(a) Evolution of the roller length L_R (m) as a function of the ratio $\frac{X_1}{h_1}$.
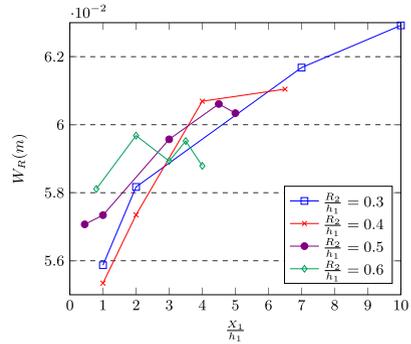
(b) Evolution of the roller width W_R (m) as a function of the ratio $\frac{X_1}{h_1}$.
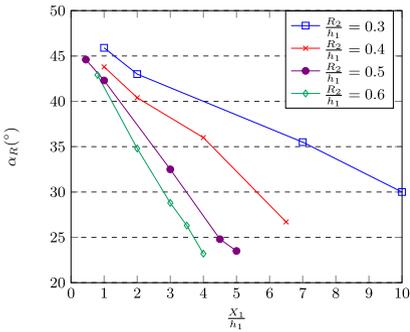
(c) Evolution of the roller angle α_R (°) as a function of the ratio $\frac{X_1}{h_1}$.
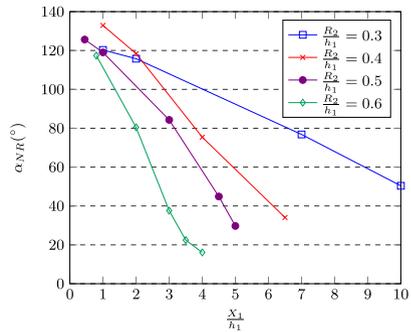
(d) Evolution of the angle of the bump inside the roller α_{NR} (°) as a function of the ratio $\frac{X_1}{h_1}$.
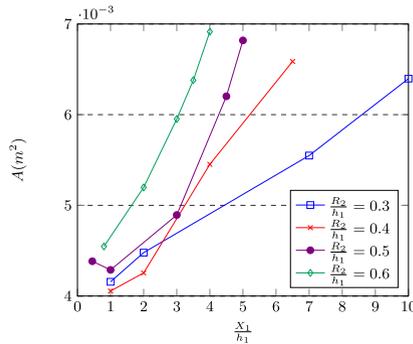
(e) Evolution of the roller area A (m^2) at the impact moment as a function of the ratio $\frac{X_1}{h_1}$.

Fig. 8 Evolution of the roller characteristics as a function of the distance between the two steps for $R_2/h_1 = 0.3$ (blue line), $R_2/h_1 = 0.4$ (red line), $R_2/h_1 = 0.5$ (purple line) and $R_2/h_1 = 0.6$ (green line) (color figure online)
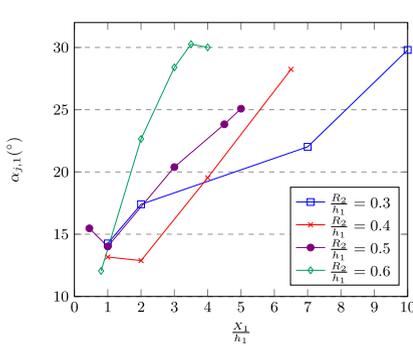
(a) Evolution of the upper jet impact angle $\alpha_{j,1}$ (°) as a function of the ratio $\frac{X_1}{h_1}$.
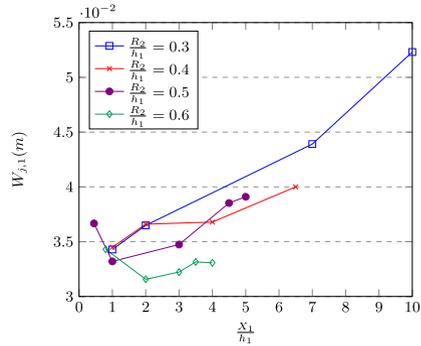
(b) Evolution of the upper jet width $W_{j,1}$ (m) as a function of the ratio $\frac{X_1}{h_1}$.
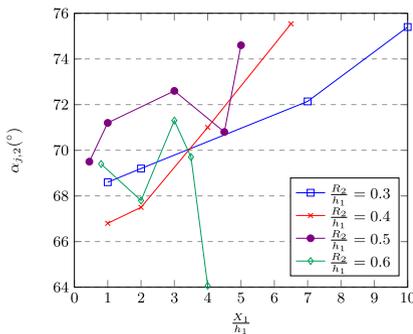
(c) Evolution of the lower jet impact angle $\alpha_{j,2}$ (°) as a function of the ratio $\frac{X_1}{h_1}$.
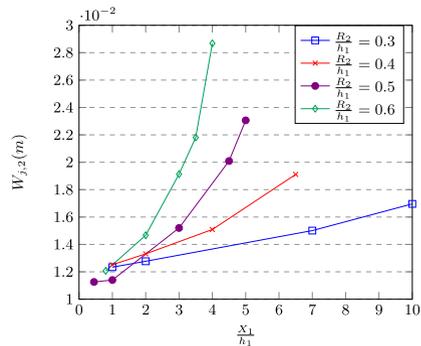
(d) Evolution of the lower jet width $W_{j,2}$ (m) as a function of the ratio $\frac{X_1}{h_1}$.

Fig. 9 Evolution of the jet characteristics at the impact moment as a function of the distance between the two steps for $R_2/h_1 = 0.3$ (blue line), $R_2/h_1 = 0.4$ (red line), $R_2/h_1 = 0.5$ (purple line) and $R_2/h_1 = 0.6$ (green line) (color figure online)

In Fig. 10a and b again for a small distance $X1$, all the results obtained are close to each other. The breaking waves with a two-crest angle $\alpha_N > -0.5°$ and a two-crest length $L_N > 0.25$ m are defined as regular breakers while the others are defined as composite breakers (see Table 4).

3.4.4 Influence of the Initial Stage on the Impacting Characteristics

The interaction between the two crests, at the beginning of the breaking event, influences the outcome of the breaking behavior. The angle between the two crests modifies the bump position inside the roller and the lower jet width (see Fig. 11). The lower the angle, the larger the jet is. The distance between the two crests has an influence on the upper jet angle and the roller length (see Fig. 12).

This demonstrates the influence of the two crests dynamic at the beginning of the breaking event on the breaking process until the impact.
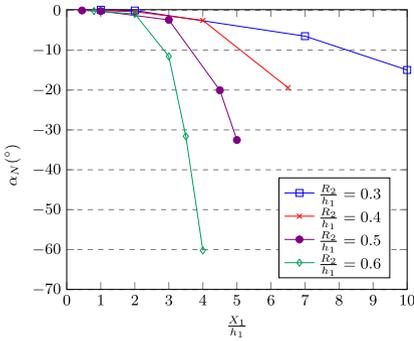
(a) Evolution of the two-crest angle α_N (°) as a function of the ratio $\frac{X_1}{h_1}$.
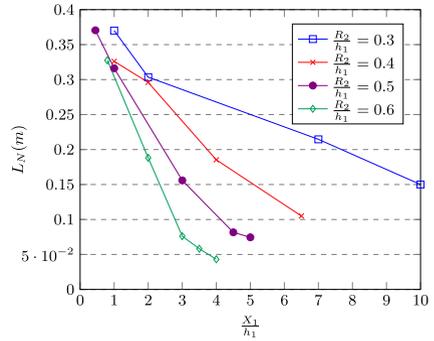
(b) Evolution of the two-crest distance L_N (m) as a function of the ratio $\frac{X_1}{h_1}$.

Fig. 10 Evolution of the two-crest characteristics at the beginning of the breaking event as a function of the distance between the two steps for $R_2/h_1 = 0.3$ (blue line), $R_2/h_1 = 0.4$ (red line), $R_2/h_1 = 0.5$ (purple line) and $R_2/h_1 = 0.6$ (green line) (color figure online)
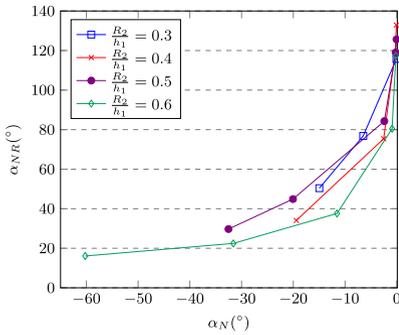
(a) Evolution of the bump angle inside the roller α_{NR} (°) as a function of the two-crest angle α_{NR} (°).
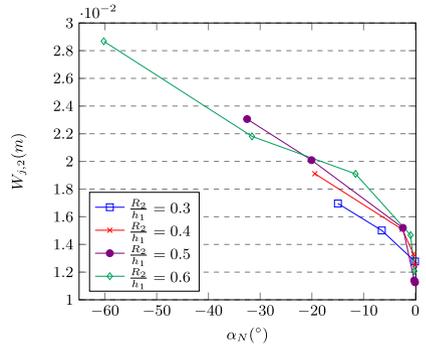
(b) Evolution of the lower jet width $W_{j,2}$ (m) as a function of the two-crest angle α_{NR} (°).

Fig. 11 Influence of the two-crest angle at the beginning of the breaking event on the angle of the bump inside the roller and the lower jet width for $R_2/h_1 = 0.3$ (blue line), $R_2/h_1 = 0.4$ (red line), $R_2/h_1 = 0.5$ (purple line) and $R_2/h_1 = 0.6$ (green line) (color figure online)

3.4.5 Summary of the Main Results

To summarize the previous results, we have observed:

(i) The interaction of the wave with each step generates a breaking event, starting with the generation of a crest. The increase of the distance X_1 or R_2 reduces the distance between the two crests. If the crests are close to each other and the first breaking event has not already turned into a plunging jet when the second one is created, a composite breaker is occurring.

(ii) During the composite breaking process, a bent on the jet is developed, creating a bump inside the roller and decomposing the jet into two unrelated jets. The
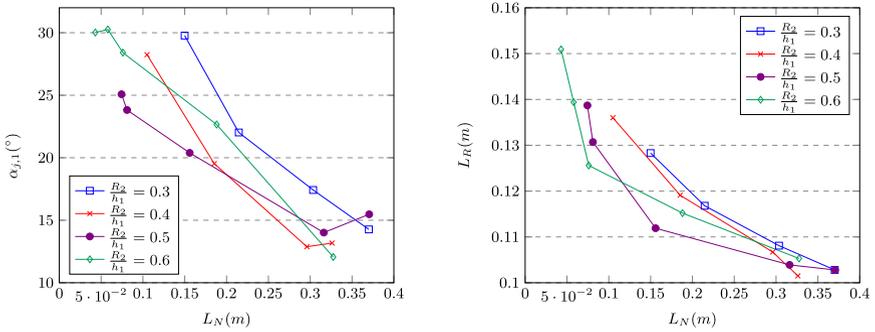
(a) Evolution of upper jet angle angle $\alpha_{j,1}$ (°) as a function of the two-crest length L_N (m).

(b) Evolution of the roller length L_R (m) as a function of the two-crest length L_N (m).

Fig. 12 Influence of the two-crest length at the beginning of the breaking event on the upper jet angle and the roller length for $R_2/h_1 = 0.3$ (blue line), $R_2/h_1 = 0.4$ (red line), $R_2/h_1 = 0.5$ (purple line) and $R_2/h_1 = 0.6$ (green line) (color figure online)

bump modifies the roller but also the jet aspects. The closer to the end of the plunging jet the bump will be, the longer and thicker the upper jet J_1 will be. Moreover, the lower jet J_2 width is influenced by the R_2 step geometry. The modification of the upper jet length, as well as the lower jet thickness, are developing the "giant" jet as defined by Yasuda et al. [55].

(iii) The composite breaker jet is falling in a farther distance than the "regular" breaking one, increasing the roller length and reducing the roller angle at the impact of the jet on the free surface.

(iv) The surface profile, distance L_N and angle α_N between the two crests, have an influence on some of the characteristics at the impact point: the bump angle inside the roller α_{NR}, the lower jet width $W_{j,2}$, the upper jet angle $\alpha_{j,1}$ and the roller length L_R.

(v) For most of our simulations, at the beginning of the breaking event, the first crest is located above the second one ($\alpha_N < 0°$).

(vi) The composite breaker roller area A is bigger than the regular breaker, which can be more than 60% higher. Thus, more air is entrapped during a composite breaking process.

4 General Discussion: Analogies with Natural Massive Waves

Yasuda et al. [55] proposed some engineering and coastal protection purposes as application for the study. But when reading the term "giant jet", as used by Yasuda et al. [55], that led us to think of some memorable natural waves, made famous for surfing and cultural culture, or for their ferocious and life-threatening aspect as Teahupo'o (Tahiti) which is a typical reef breaking wave, which, in certain conditions, can lead to a world-famous massive surfing wave. As shown in the video footage made by Bryan [6] where we can see some examples of Teahupo'o at its biggest ever filmed

(as advertised!). What can be seen in the proposed video, was filmed on the 27th of August, 2011, of what many are calling the biggest Teahupo'o ever ridden. Chris Bryan, internationally renown photographer, was fortunate to be able to work for Billabong (host of the surfing event) on a day that is remembered in the history of big wave surfing. The French Navy labeled this day a double red code, prohibiting and threatening to arrest anyone that entered the water. There have arguably been more moments like this one at Teahupo'o than at any other single surf spot on the planet, outside Pipeline (Hawaii, USA). The "Right" is also one of the world's most formidable and dangerous waves, located near Walpole (south of Perth) in Western Australia. As thick as it is high, the Right is notoriously difficult to surf, endangering anyone who attempts to surf it. Like other "slab waves" around the world (Mavericks in California, USA, for example), this famous wave owes much of its famous form to underwater bathymetry. It also combines the swell sources and the winds to produce this picturesque breaking wave, but as discussed in the following, the work of Yasuda et al. [55] allows providing some insight to explain the formation of such spectacular waves.

When you go through the literature and online documentaries associated with surfing culture and more particularly dedicated to the description of the breaking waves encountered in the four corners of the globe, from the local spot to the "secret spot" via the most recommended spots, you come across many qualifiers and superlatives used to qualify and romanticize the descriptions while trying to describe as accurately as possible the qualities and characteristics of each wave. Whether discussing esthetic, spectacular aspects or technical details dedicated to the practice of surfing, we can find elements indicating the size or speed, the frequency and the preferential conditions of appearance of the best breaking waves allowing to offer the best surfing experience, the potential danger of a site in which the waves break, we even find qualifiers indicating the fury, the ugliness, the intensity, the fierceness, and the aggressiveness of some waves, even leading people to coin the waves or places with qualifiers leaving no doubt about the interpretation that the observers wanted to give (Jaws, for example, in North Shore of the island of Maui, Hawaii, Cape Fear also known as Devil's Point, in Shipstern Bluff located on the southern point of the Tasman Peninsular in Tasmania, Australia, etc.). Scales and levels are even proposed in the descriptions to identify the appropriate technical level for any practitioner. Some elements of description use qualifiers to depict the sound generated by the breaking waves: the waves are described as roaring, loud and noisy, crashing tumultuously, etc. The appearance is sometimes described as gorgeous or beautiful, but sometimes these unusual breaking waves are described as horrifying, mutant, hideous, monstrous, sometimes freakish, emphasizing the disturbing, unusual and unpredictable nature of these breaking waves, leaving the explanations as mysterious or revealing the complexity or power of Nature. The external conditions of the occurrence of these specific conditions are usually well known (swell and wind directions, swell height, angle and period, etc.), but the exact nature of the bathymetry is not known in details and more specifically, the reasons why the breaking waves exhibit such characteristics are not fully understood.

The objective of many scientific works has therefore been to try to answer the following question: how to list or parameterize characteristics such as intensity, geometry, power, strength, and energy of breaking waves, with a more practical and technical

than esthetic purpose, then how to organize, classify and calibrate these indexes or scales and how to estimate the values of these parameters? What is a violent or dangerous wave? How to design coastal or harbor infrastructures to protect sites according to their use and to the conditions to which they are subjected by breaking waves?

4.1 Abrupt Change in Depth

The so-called "traditional" waves, whether they break on sand or reef, usually rise gradually when they propagate over a gradually varying changing bathymetry. The incident waves coming offshore progressively advance before bending their direction and slowing down as they get closer to the shore, swelling up to a critical point, the breaking point, which is visually identified when the front face of the steepening wave is almost vertical. What the surfing community identifies as a "slab wave", the swell moving in deep water does not slow at all. Thus, it retains almost all of its energy until it hits a shallow seabed, whether it is at the foot of a cliff or hundreds of meters away from the coast. Suddenly pushed upwards, the wave transforms into a formidable wall of water (sometimes several meters high). At the same time, the bottom of the wave sucks in water from the shallower part of the bathymetry and deepens in such a way that it can break below sea level.

This is the case of a slab wave identified at a spot called Scott's Reef (United States), whose rock bathymetry bottom goes from about thirty meters to 10 m or even less than a meter depending on the tide. Or the breaking wave coined "Ours" (Botany Bay, Cape Solander, located South Sydney in Australia), which goes from 26 m to two or even less than a meter depending on the tide.

This feature is similar to what we discussed previously in the configuration of the double-step reef. the solitary wave encountered two abrupt changes of bathymetry, modeled by the two successive steps, this led to the formation of a composite breaker.

4.2 Change of Form

Once the wave reaches the slab, it follows its shape. Thus, the wave can take a deformed shape, like Shipstern's Bluff (Tasmania, Australia) and the steps caused by the brutal change of bathymetry of the reef which deform the "curl" of the wave. Or like "Ours" (Australia) and its plunging jet capable of splitting or even tripling. This aspect is found in our numerical results (see Fig. 2c, and discussed by Yasuda et al. [55], where some of the waves are observed to break multiple times. On the contrary, other slab waves are distinguished by their perfection. Like Teahupo'o and its well-ordered coral reef that shapes a perfect wave, breaking with a noticeable regularity. When looking at the breaking line from above, a general horseshoe form is observed as the breaking front line wraps around a curved coral head. this situation probably corresponds to what we described when the distance X_1 was short and both heights R_1 and R_2 were adequate to generate the perfect timing between the crest–crest exchange to lead to a "giant plunging jet".

4.3 Bursting of the Main Air Cavity

When waves break, the plunging jets envelop a large quantity of air, often referred to as a tube. So usually slab waves are not described as breaking, but they rather explode, due to the size of the plunging jets and the speed of the collapsing tube of air. The waves that come from the open sea do not shift, and sometimes it is impossible to see the wave coming before it breaks on the rock. This is why the bursting of a slab wave is short, powerful and very intense. This is also observed from our numerical results, when a larger pocket of air is entrapped, before bursting as it is compressed by a large amount of water pushing, and the very shallow location of the plunge impact.

5 Conclusions and Perspectives

While working on the verification and validation of our numerical tool [11, 12], we came across some somehow uncited experimental results, discussing a "new type of breaker". The experimental configuration involve an easy and controlled initial setup geometry, which allows checking that our numerical tool could reproduce the breaking characteristics when comparing experimental and numerical results.

We investigated the new type of breaker, proposed by Yasuda et al. [55], by detailing several aspects which lead to the unusual size and behavior of some plunging jets generated when waves break above some drastic changes of bathymetry. We thoroughly investigated all geometrical aspects of the breaking process, to propose a classification of the breaker types which were observed in our numerical results. We indicated the influences of the reef parameters (steps heights and lengths) on the subsequent breaking process. We also showed that the air entrainment was indeed much larger during the composite breaker occurrence.

As discussed in the last section of the article, all the aspects found in massive natural breaking waves are addressed in the work of Yasuda et al. [55] and Yasuda et al. [54], rooting from the early study from Cooker et al. [8]. They highlighted that abrupt underwater modifications consisting in multiple stages, as it is the case with the use of a double reef, trigger an instability which will later participate in the generation of larger than usual plunging breaker. It has even been shown that the multi-crest composition, when at breaking point, could explain the aspect of some natural waves to be described as splitting or even tripling at the jet ejection, as mentioned earlier. It was also observed that larger quantities of air were entrapped during the breaking process, with very high splash-ups.

As described before, some waves are observed to break below sea level, due to the suction effect of the water from the shallower top of the bathymetry. Unfortunately, we did not notice this feature when using solitary waves, as the water cannot retreat offshore from a previous breaking wave. Thus, in order to go more into details, it would be needed to study periodic waves, but, as a preliminary work, we chose to use solitary waves, for the sake of simplicity and for comparisons matter with the observations from Yasuda et al. [55] and Yasuda et al. [54]. This paper is also a call for experimental results on the particular use of a double reef, to investigate and compare the triggering and further evolution of the instability, as well as the three-dimensional

aspects. Checking the speed and timing of all the processes would also be appreciable, as it would be the subject of future investigation.

Data Availability Statement Movies and pictures generated from the numerical simulations can be made available on reasonable request. The numerical tool used to generate the simulations is an open-source tool, available from: https://notus-cfd.org/. Source code available from: https://git.notus-cfd.org/notus/notus.

Declarations

Conflict of interest On behalf of all the authors, the corresponding author states that there is no conflict of interest.

References

1. Bacigaluppi, P., Ricchiuto, M., Bonneton, P.: Implementation and evaluation of breaking detection criteria for a hybrid boussinesq model. Water Waves **2**, 207–241 (2020)
2. Battjes, J.A.: Surf-zone dynamics. Ann. Rev. Fluid Mech. **20**, 257–293 (1988)
3. Blenkinsopp, C.E., Chaplin, J.R.: Void fraction measurements in breaking waves. Proc. R. Soc. A Math. Phys. Eng. Sci. **463**(2088), 3151–3170 (2007)
4. Blenkinsopp, C.E., Chaplin, J.R.: The effect of relative crest submergence on wave breaking over submerged slopes. Coast. Eng. **55**(12), 967–974 (2008)
5. Brackbill, J.U., Kothe, D.B., Zemach, C.: A continuum method for modeling surface tension. J. Comput. Phys. **100**(2), 335–354 (1992)
6. Bryan, C.: Biggest teahupoo ever, shot on the phantom camera. All images were shot by Chris Bryan using the Phantom HD Gold camera. WWW.CHRISBRYANFILMS.COM. Video available via Youtube: https://www.youtube.com/watch?v=7woVTuN8k3c (2011)
7. Chang, K.-A., Hsu, T.-J., Liu, P.L.-F.: Vortex generation and evolution in water waves propagating over a submerged rectangular obstacle. Coast. Eng. **44**, 13–36 (2001)
8. Cooker, M.J., Peregrine, D.H., Vidal, C., Dold, J.W.: The interaction between a solitary wave and a submerged semicircular cylinder. J. Fluid Mech. **215**, 1–22 (1990)
9. Deborde, J., Milcent, T., Lubin, P., Glockner, S.: Simulations of the interaction of solitary waves and elastic structures with a fully Eulerian method. Water Waves **2**, 433–466 (2020)
10. Deike, L.: Mass transfer at the ocean–atmosphere interface: the role of wave breaking, droplets, and bubbles. Ann. Rev. Fluid Mech. **54**(1), 191–224 (2022)
11. Desmons, F.: étude numérique du déferlement de vagues capillo-gravitaires. Ph.D. thesis, Université de Bordeaux, retrieved from https://tel.archives-ouvertes.fr/tel-03204107 (2021)
12. Desmons, F., Coquerelle, M.: A generalized high-order momentum preserving (homp) method in the one-fluid model for incompressible two phase flows with high density ratio. J. Comput. Phys. **437**, 110322 (2021)
13. Galvin, C.J.: Breaker type classification on three laboratory beaches. J. Geophys. Res. **73**, 3651–3659 (1968)
14. Goda, K.: A multistep technique with implicit difference schemes for calculating two- or three-dimensional cavity flows. J. Comput. Phys. **30**(1), 76–95 (1979)
15. Gourlay, M.R.: Wave transformation on a coral reef. Coast. Eng. **23**(1), 17–42 (1994)

16. Gourlay, M.R.: Wave set-up on coral reefs. 1. set-up and wave-generated flow on an idealised two dimensional horizontal reef. Coast. Eng. **27**(3), 161–193 (1996)
17. Gourlay, M.R.: Wave set-up on coral reefs. 2. set-up on reefs with various profiles. Coast. Eng. **28**(1), 17–55 (1996)
18. Gourlay, M.R., Colleter, G.: Wave-generated flow on coral reefs-an analysis for two-dimensional horizontal reef-tops with steep faces. Coast. Eng. **52**(4), 353–387 (2005)
19. Hara, M., Yasuda, T., Sakakibara, Y.: Characteristics of a solitary wave breaking caused by a submerged obstacle. Coast. Eng. Proc. **1**(23), 253–266 (1992)
20. Helluy, P., Gollay, F., Grilli, S.T., Seguin, N., Lubin, P., Caltagirone, J.-P., Vincent, S., Drevard, D., Marcer, R.: Numerical simulations of wave breaking. Math. Model. Numer. Anal. **39**(3), 591–608 (2005)
21. Hsiao, S.-C., Lin, T.-C.: Tsunami-like solitary waves impinging and overtopping an impermeable seawall: experiment and rans modeling. Coast. Eng. **57**, 1–18 (2010)
22. Huang, C.-J., Chang, H.-H., Hwung, H.-H.: Structural permeability effects on the interaction of a solitary wave and a submerged breakwater. Coast. Eng. **49**(1), 1–24 (2003)
23. Kalisch, H., Ricchiuto, M., Bonneton, P., Colin, M., Lubin, P.: Introduction to the special issue on breaking waves. Eur. J. Mech. B Fluids **73**, 1–5 (2019)
24. Kazolea, M., Delis, A.I., Synolakis, C.E.: Numerical treatment of wave breaking on unstructured finite volume approximations for extended boussinesq-type equations. J. Comput. Phys. **271**, 281–305 (2014)
25. Kazolea, M., Ricchiuto, M.: On wave breaking for boussinesq-type models. Ocean Model. **123**, 16–39 (2018)
26. Kiger, K.T., Duncan, J.H.: Air-entrainment mechanisms in plunging jets and breaking waves. Ann. Rev. Fluid Mech. **44**, 563–596 (2012)
27. Lee, J.-J., Skjelbreia, J.E., Raichlen, F.: Measurements of velocities in solitary waves. J. Waterw. Port Coast. Ocean Div. **WW2**(108), 200–218 (1982)
28. Liu, P.L.-F., Cheng, Y.: A numerical study of the evolution of a solitary wave over a shelf. Phys. Fluids **13**(6), 1660–1667 (2001)
29. Losada, M.A., Vidal, C., Medina, R.: Experimental study of the evolution of a solitary wave at an abrupt junction. J. Geophys. Res. Oceans **94**(C10), 14557–14566 (1989)
30. Lubin, P.: Large eddy simulation of plunging breaking waves. Ph.D. thesis, Université Bordeaux I, in English (2004)
31. Lubin, P., Chanson, H.: Are breaking waves, bores, surges and jumps the same flow? Environ. Fluid Mech. **17**, 47–77 (2017)
32. Lubin, P., Chanson, H., Glockner, S.: Large eddy simulation of turbulence generated by a weak breaking tidal bore. Environ. Fluid Mech. **10**(5), 587–602 (2010)
33. Lubin, P., Glockner, S.: Numerical simulations of three-dimensional plunging breaking waves: generation and evolution of aerated vortex filaments. J. Fluid Mech. **767**, 364–393 (2015)
34. Lubin, P., Glockner, S., Kimmoun, O., Branger, H.: Numerical study of the hydrodynamics of regular waves breaking over a sloping beach. Eur. J. Mech. B Fluids **30**(6), 552–564 (2011)
35. Lubin, P., Lemonnier, H.: Propagation of solitary waves in constant depths over horizontal beds. Multiph. Sci. Technol. **16**(1–3), 237–248 (2004)
36. Lubin, P., Vincent, S., Abadie, S., Caltagirone, J.-P.: Three-dimensional large eddy simulation of air entrainment under plunging breaking waves. Coast. Eng. **53**(8), 631–655 (2006)
37. Lubin, P., Vincent, S., Caltagirone, J.-P.: On the Navier–Stokes equations simulation of the head-on collision between two surface solitary waves. C. R. Mécanique **333**(4), 351–357 (2005)
38. Massel, S.R., Gourlay, M.R.: On the modelling of wave breaking and set-up on coral reefs. Coast. Eng. **39**(1), 1–27 (2000)
39. Mayer, R.H., Kriebel, D.L.: Wave runup on composite-slope and concave beaches. In: Proceedings of 24th International Conference Coastal Engineering, pp. 2325–2339 (1994)
40. Mutsuda, H., Yasuda, T.: Numerical simulation of turbulent air-water mixing layer within surf-zone. In: Proceedings of 27th International Conference Coastal Engineering, pp. 755–768 (2000)
41. Owkes, M., Desjardins, O.: A mesh-decoupled height function method for computing interface curvature. J. Comput. Phys. **281**, 285–300 (2015)
42. Peregrine, D.H.: Breaking waves on beaches. Annu. Rev. Fluid Mech. **15**, 149–178 (1983)
43. Popinet, S.: An accurate adaptive solver for surface-tension-driven interfacial flows. J. Comput. Phys. **228**(16), 5838–5866 (2009)
44. Popinet, S.: Numerical models of surface tension. Ann. Rev. Fluid Mech. **50**(1), 49–75 (2018)

45. Robertson, B., Hall, K., Zytner, R., Nistor, I.: Breaking waves: review of characteristic relationships. Coast. Eng. J. **55**(1), 13500021–135000240 (2013)
46. Seabra-Santos, F.J., Renouard, D.P., Temperville, A.M.: Numerical and experimental study of the transformation of a solitary wave over a shelf or isolated obstacle. J. Fluid Mech. **176**, 117–134 (1997)
47. Svendsen, I.A.: Analysis of surf zone turbulence. J. Geophys. Res. **92**(C5), 5115–5124 (1987)
48. Svendsen, I.A., Putrevu, U.: Surf-zone Hydrodynamics, Advances in Coastal and Ocean Engineering, vol. 2, pp. 1–78. World Scientific, Singapore (1996)
49. Whitam, G.B.: Linear and Non-linear Waves. Wiley-Interscience Publication, New York (1974)
50. Wroniszewski, P.A., Verschaeve, C.G.J., Pedersen, K.G.: Benchmarking of Navier–Stokes codes for free surface simulations by means of a solitary wave. Coast. Eng. **91**, 1–17 (2014)
51. Xu, J.Y., Liu, S.X., Li, J.X., Jia, W.: Experimental study of wave propagation characteristics on a simplified coral reef. J. Hydrodyn. **32**, 385–397 (2020)
52. Yasuda, T., Hara, M.: Breaking and reflection of a steep solitary wave caused by a submerged obstacle. Coast. Eng. Proc. 1(22), 923–934 (1990)
53. Yasuda, T., Mutsuda, H., Mizutani, N.: Kinematics of overturning solitary waves and their relations to breaker types. Coast. Eng. **29**, 317–346 (1997)
54. Yasuda, T., Mutsuda, H., Mizutani, N., Matsuda, H.: Relationships of plunging jet size to kinematics of breaking waves with spray and entrained air bubbles. Coast. Eng. J. **41**(2), 269–280 (1999)
55. Yasuda, T., Mutsuda, H., Oya, A., Tada, A., Fukumoto, T.: A new type breaker forming a giant jet and its decaying properties. In: Proceedings 25th International Conferences Coastal Engineering, pp. 300–313 (1996)